Orissa Journal of Physics
ISSN 0974-8202

Vol. 26, No.2
August 2019
pp. 107-128

Darcy-Forchheimer slip flow of Fe_3O_4–$(CH_2OH)_2$ nanofluid due to a permeable rotating disk

M K NAYAK

Department of Physics, IHSE, Siksha "O" Anusandhan Deemed to be University, Bhubaneswar-751003, Odisha, India

Corresponding author. Email: mkn2122@gmail.com

Received: 10.06.2019 ; *Revised : 9.07.2019* ; *Accepted : 2.08.2019*

Abstract: The influence of velocity slip and suction on Darcy-Forchheimer flow of $Fe_3O_4-(CH_2OH)_2$ nanofluid past stretching/shrinking rotating disk subject to convective boundary condition has been investigated in the current study. The similarity transformations are implemented to establish the non dimensional governing non linear equations. Numerical solutions of such system of eqution are developed by robust fourth order Runge Kutta method along with shooting technique. The relevant outcomes of the present study are that more and more slip peters out the tangential velocity while fluid suction undermines the radial velocity of Darcy-Forchheimer flow of $Fe_3O_4-(CH_2OH)_2$ nanofluid due to stretching/shrinking rotating disk. In addition, convective heat transfer strengthens viscous drag force and peters out heat transfer rate from the surface of both stretching and shrinking rotating disks.

Keywords: Iron oxide-ethylene glycol $[Fe_3O_4-(CH_2OH)_2]$ nanofluid; Darcy-Forchheimer flow; Velocity slip; Suction.

1. Introduction

In the past decades, conventional fluids such as water, kerosene, ethylene glycol, engine oil etc. were used as coolants for the needs of the industrial and manufacturing sectors. However, such fluids could not meet the desired cooling requirements of the ever expanding modern industrial world. Considering such pitfalls into mind, Choi [1] was a pioneer to experimentally found a novel type of fluid named as nanofluid in 1995 at Argonne National Laboratory, USA. The nanofluids are formed through proper dilution and suspension of nanoparticles [nano meter-sized particles (smaller than 100 nm)] such as copper (Cu), nickel

(Ni), aluminium (Al), Silver (Ag), titanium oxide (TiO_2), aluminium oxide (Al_2O_3), copper oxide (CuO), iron oxide (Fe_3O_4), silicon carbide (SiC), zinc carbide (ZNC), carbon nanotubes, nano rods, etc. with the base fluids/conventional fluids. Insertion of nanoparticles into base fluids appreciably enhances the thermal conductivity (heat transfer performance) of base fluids so as to cater the cooling as one of the technical challenges faced in numerous industries.

Nanofluids have many applications in environmental technology, heating control systems, chemical industry, storage of energy, energy generation, combustion, heat exchangers, micro-channel heat sinks, thermal absorption, electronics cooling, transformer cooling, computers cooling, vehicle cooling, heavy-duty engine cooling, processing of energy, nuclear reactors, microelectronics, refrigeration, automotives, design of the waste heat removal equipment, aircrafts and space applications, high energy devices, manufacturing (of oil and gas, food and drink, paper and printing), polymer extrusion, glass blowing, rapid spray cooling, wire drawing and quenching in metal foundries, refrigerant to chill or cool buildings and many others. Moreover, nanofluids are used to develop the best quality lubricants and oils and also as cooling agent in industries to enhance the efficiency, save energy and reduce emissions. Especially the magneto nanofluids are useful in magnetohydrodynamic (MHD) pumps and accelerators, MHD power generators, cancer therapy, removal of blockage in the arteries, safer surgery, asthma treatment, targeted drug release/drug delivery, elimination of tumors with hyperthermia, wound treatment, sterilized devices, biomedicine, antibacterial treatment, magnetic resonance imaging etc.

In the face of such relevance and widespread applications, many researchers have been attracted and therefore carried out their investigations in the related areas. For instance, magnetohydrodynamic boundary layer flow of a Maxwell nanofluid over a stretching sheet was studied by Afify and Elgazery [2], Joule heating and viscous dissipation effect on the flow of nanofluids past a rotating disk was analyzed by Hayat et al. [3], three dimensional free convective MHD flow of nanofluid over permeable linear stretching sheet with thermal radiation was discussed by Nayak et al. [4], the flow of third grade nanofluid due to rotating stretchable disk subject to chemical reaction and heat source was studied by Hayat et al. [5], MHD 3D flow and heat transfer analysis of nanofluid by shrinking surface inspired by thermal radiation and viscous dissipation was

examined by Nayak [6], impact of Cattaneo-Christov heat flux on MHD nanofluid flow and heat transfer between parallel plates associated with thermal radiation was investigated by Dogonchi and Ganji [7] and magnetohydrodynamic flow and heat transfer impact on ZnO-SAE50 nanolubricant flow due to an inclined rotating disk was studied by Nayak et al. [8].

The no-slip boundary condition is known as the main manifestation of the Navier-Stokes theory of fluid dynamics. In certain situations, the assumption of no-slip boundary condition does no longer apply. In micro-scale fluid dynamics involving micro-scale dimensions, the flow behavior of fluids is usually associated with slip flow regime and different from traditional flow. For instance, when fluid flows in micro electrical mechanical systems (MEMS), the no-slip condition at the solid fluid interface is no longer applicable. Further, no slip boundary condition is inadequate in the situations viz. polymer solutions, suspensions, emulsions and foams (where fluid behaves as a particulate), therefore, the appropriate boundary condition is the partial slip. In such aspects, a partial slip may occur on a stationary and moving boundary. A slip flow model more accurately describes the non-equilibrium near the interface. In view of its important role in polymer and electrochemical industry, many authors have studied the flow analysis in association with partial slip condition. MHD nanofluid flow over a rotating disk with partial slip effects using Buongiorno model was analyzed by Mustafa [9] and effect of slip on MHD 3D stretched flow of nanofluid through porous media inspired by non-linear thermal radiation was examined by Nayak et al. [10].

The flow and heat transfer over rotating disk finds many important applications include geothermal and geophysical systems, aerospace engineering, storage devices, medical instruments, crystal growing, and food processing technologies. Von Kármán [11] revealed the nature of flow induced by stretched rotating disk. A numerical investigation of viscous flow due to a porous disk was carried out by Turkyilmazoglu and Senel [12]. Boundary layer approximations to a rotating flow due to a disk was pioneered by Bödewadt [13]. Sheikholeslami et al. [14] discussed the nanofluid spraying on an inclined rotating disk for cooling process.

In fact, flows through a permeable media are vital in hydrology, geothermal energy systems, petroleum reservoirs, crude oil and gas production, heat exchangers, food processing, electro chemistry, catalytic reactors, fermentation process, water movement in reservoirs etc. [15-16]. The classical Darcy's law is not implementable for a non-linear fluid flow in a porous medium. In such

environment, inertia and boundary features cannot be ignored. In case of high velocities, Reynolds number (depends upon the pore size) is greater than unity. In order to exhibit the inertia and boundary features, Forchheimer [17] supplemented a square velocity factor to the Darcian velocity in the associated momentum equation. Moreover, Muskat [18] declared this factor as "Forchheimer term" which is always valid for a large Reynolds number**.** Influence of viscous dissipation and thermophoresis on Darcy- Forchheimer mixed convection in a fluid saturated porous media was analyzed by Seddeek [19]. Further, Cattaneo-Christov heat flux model for Darcy-Forchheimer flow of an Oldroyd-B fluid with variable conductivity and non-linear convection was examined by Shehzad et al. [20].

Nomenclature

(u, v, w) velocity components in increasing (r, ϕ, z) directions $\left(m\,s^{-1}\right)$

ρ_{nf} effective density of the nanofluid $\left(kg\,m^{-3}\right)$

ρ_s density of solid nanoparticles $\left(kg\,m^{-3}\right)$

ρ_f density of base fluid $\left(kg\,m^{-3}\right)$

$\left(\rho C_p\right)_{nf}$ heat capacitance of the nanofluid $\left(J\,kg^2\,m^3K^{-1}\right)$

$\left(\rho C_p\right)_f$ heat capacitance of base fluid $\left(J\,kg^2\,m^3K^{-1}\right)$

$\left(\rho C_p\right)_s$ heat capacitance of solid nanoparticles $\left(J\,kg^2\,m^3K^{-1}\right)$

μ_{nf} effective dynamic viscosity of the nanofluid $\left(kg\,m^{-1}s^{-1}\right)$

μ_f effective dynamic viscosity of base fluid $\left(kg\,m^{-1}s^{-1}\right)$

μ_s effective dynamic viscosity of base fluid $\left(kg\,m^{-1}s^{-1}\right)$

β_{nf} thermal expansion of nanofluid $\left(K^{-1}\right)$

β_f thermal expansion of base fluid $\left(K^{-1}\right)$

β_s thermal expansion of nanoparticle $\left(K^{-1}\right)$

k_{nf} thermal conductivity of nanofluid $\left(W\ m^{-1}K^{-1}\right)$

k_f thermal conductivity of base fluid $\left(W\ m^{-1}K^{-1}\right)$

k_s thermal conductivity of nanoparticle $\left(W\ m^{-1}K^{-1}\right)$

α_f thermal diffusivity of the base fluid $\left(m^2s^{-1}\right)$

T_w surface temperature $\left(K\right)$

T_f temperature of heated fluid $\left(K\right)$

T fluid temperature in the boundary layer $\left(K\right)$

T_∞ Ambient fluid temperature $\left(K\right)$

L_1 wall slip coefficient

h_f heat transfer coefficient $\left(Wm^{-2}K^{-1}\right)$

$K=\dfrac{\upsilon_f}{\gamma K^*}$ porosity parameter p pressure $\left(Pa\right)$

$G_r=\dfrac{g\beta_f\left(T_f-T_\infty\right)r^3}{\upsilon_f^2}$ thermal Grassof number $\Upsilon=\dfrac{W}{\sqrt{2\Omega\upsilon_f}}$ suction parameter

K^* permeability of porous medium ϕ solid volume fraction

$\Pr=\dfrac{\nu_f}{\alpha_f}$ Prandtl number $\mathrm{Re}=\dfrac{\Omega R^2}{\upsilon_f}$ rotational Reynolds number

$\gamma=\dfrac{s}{\Omega}$ stretching strength parameter $\Gamma=L_1\mu_f\sqrt{\dfrac{2\Omega}{\upsilon_f}}$ wall slip parameter

$F_r=\dfrac{C_d}{\sqrt{K^*}}$ inertia coefficient $B_i=\dfrac{h_f}{k_f}\sqrt{\dfrac{\upsilon_f}{2\Omega}}$ Biot number

$F^*\left(=\dfrac{C_d}{rK^{*1/2}}\right)$ non-uniform inertia coefficient C_d drag coefficient

f base fluid *W* suction velocity

nf nanofluids *s* nano solid particles

From the above literature survey we observe that a very few work has been carried out regarding the Darcy- Forchheimer flow past a rotating disk. However, Darcy- Forchheimer slip flow due to a rotating disk is yet to be done. Therefore, our objective is to study the effect of velocity slip on the flow of

$Fe_3O_4-(CH_2OH)_2$ nanofluid past a stretching/shrinking rotating disk subject to suction and convective boundary condition.

2. Physical Model

We consider a steady incompressible Darcy-Forchheimer flow of $Fe_3O_4-(CH_2OH)_2$ nanofluid due to a stretching/shrinking rotating disk subject to velocity slip, suction and convective boundary condition. In present study, $(CH_2OH)_2$ or pure water is considered as base fluid Fe_3O_4 is taken as nanoparticle. The disk at z=0 spins with constant angular velocity Ω. The velocity components (u,v,w) are in the directions of increasing (r,ϕ,z) respectively [Fig.1].

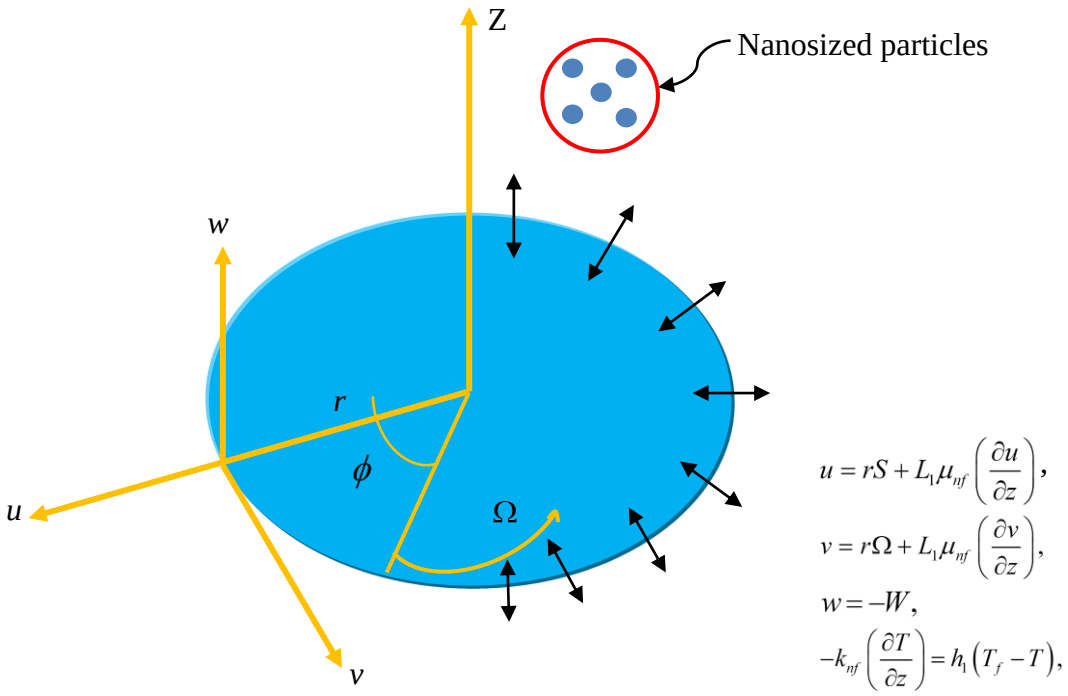

Fig. 1: Flow geometry

The governing equations for the flow due to a rotating disk are:

$$\frac{\partial u}{\partial r}+\frac{u}{r}+\frac{\partial w}{\partial z}=0\,, \tag{1}$$

$$u\frac{\partial u}{\partial r}-\frac{v^2}{r}+w\frac{\partial u}{\partial z}=-\frac{1}{\rho_{nf}}\frac{\partial p}{\partial r}+\frac{\mu_{nf}}{\rho_{nf}}\left(\frac{\partial^2 u}{\partial r^2}+\frac{1}{r}\frac{\partial u}{\partial r}-\frac{u}{r^2}+\frac{\partial^2 u}{\partial z^2}\right) + \frac{(\rho\beta)_{nf}}{\rho_{nf}}g\left(T-T_\infty\right)-\frac{\mu_{nf}}{\rho_{nf}}\frac{u}{K^*}-F^*u^2\,, \tag{2}$$

$$u\frac{\partial v}{\partial r}+\frac{uv}{r}+w\frac{\partial v}{\partial z}=\frac{\mu_{nf}}{\rho_{nf}}\left(\frac{\partial^2 v}{\partial r^2}+\frac{1}{r}\frac{\partial v}{\partial r}-\frac{v}{r^2}+\frac{\partial^2 v}{\partial z^2}\right) + \frac{(\rho\beta)_{nf}}{\rho_{nf}}g\left(T-T_\infty\right)-\frac{\mu_{nf}}{\rho_{nf}}\frac{v}{K^*}-F^*v^2\,, \tag{3}$$

$$u\frac{\partial w}{\partial r}+w\frac{\partial w}{\partial z}=-\frac{1}{\rho_{nf}}\frac{\partial p}{\partial z}+\frac{\mu_{nf}}{\rho_{nf}}\left(\frac{\partial^2 w}{\partial r^2}+\frac{1}{r}\frac{\partial w}{\partial r}+\frac{\partial^2 w}{\partial z^2}\right), \tag{4}$$

$$u\frac{\partial T}{\partial r}+w\frac{\partial T}{\partial z}=\frac{k_{nf}}{\left(\rho C_p\right)_{nf}}\left(\frac{\partial^2 T}{\partial r^2}+\frac{1}{r}\frac{\partial T}{\partial r}+\frac{\partial^2 T}{\partial z^2}\right) \tag{5}$$

With appropriate boundary conditions:

$$\left.\begin{aligned} u=rS+L_1\mu_{nf}\left(\frac{\partial u}{\partial z}\right),\ v=r\Omega+L_1\mu_{nf}\left(\frac{\partial v}{\partial z}\right),\ w=-W,\\ -k_{nf}\left(\frac{\partial T}{\partial z}\right)=h_f\left(T_f-T\right)\ \ at\ \ z=0\\ u\to 0,\ v\to 0, T\to T_\infty,\ p\to p_\infty\ \ \ as\ \ z\to\infty \end{aligned}\right\} \tag{6}$$

where u, v, w are the velocity components in increasing r, ϕ, z directions respectively, p is the pressure within the boundary layer, K^* permeability of the medium, F^* is the non-uniform inertia coefficient, p_∞ is the pressure of the ambient fluid, T is the temperature of the fluid within the boundary layer, S is the stretching/shrinking rate of the disk. Here, $S>0$ indicates stretching rotating disk while $S<0$ indicates shrinking rotating disk, T_∞ is the ambient fluid

temperature, h_f is the heat transfer coefficient, L_1 is the wall slip coefficient and W is the suction velocity.

The effective density and heat capacitance of the nanofluid are defined as

$$\left.\begin{aligned}\rho_{nf} &= (1-\phi)\rho_f + \phi\rho_s \\ (\rho C_p)_{nf} &= (1-\phi)(\rho C_p)_f + \phi(\rho C_p)_s\end{aligned}\right\} \tag{7}$$

Where ρ_{nf} is the effective density of the nanofluid, ρ_s is the density of solid nanoparticles, ρ_f is the density of base fluid, $\left(\rho C_p\right)_{nf}$ is the heat capacitance of the nanofluid, $\left(\rho C_p\right)_f$ is the heat capacitance of base fluid, $\left(\rho C_p\right)_s$ is the heat capacitance of solid nanoparticles and ϕ is the solid volume fraction.

The effective dynamic viscosity of the nanofluid is defined as

$$\mu_{nf} = \frac{\mu_f}{(1-\phi)^{2.5}} \tag{8}$$

where μ_{nf} is the effective dynamic viscosity of the nanofluid, μ_f is the effective dynamic viscosity of base fluid and μ_s is the effective dynamic viscosity of nanoparticles.

The thermal expansion of nanofluid is

$$(\rho\beta)_{nf} = (1-\phi)(\rho\beta)_f + \phi(\rho\beta)_s \tag{9}$$

Where β_{nf} , β_f and β_s are the thermal expansion of nanofluid, base fluid and nanoparticles respectively.

Following the model proposed by Maxwell-Granett, the effective thermal conductivity of nanofluid can be determined as

$$\frac{k_{nf}}{k_f} = \frac{\left(k_s + 2k_f\right) - 2\phi\left(k_f - k_s\right)}{\left(k_s + 2k_f\right) + \phi\left(k_f - k_s\right)} \tag{10}$$

where k_{nf} , k_f and k_s are respectively the thermal conductivities of nanofluids, base fluids and nanoparticles respectiviley.

The transformations necessitated for the present problem include:

$$\left.\begin{aligned}(u,v,w)&=\left(r\Omega F'(\eta),r\Omega G(\eta),-\sqrt{2\Omega\upsilon_f}\,F(\eta)\right)\\(p,T)&=\left(p_\infty-\Omega\mu_f P(\eta),\,T_\infty+\left(T_f-T_\infty\right)\theta\right)\\\eta&=\sqrt{\frac{2\Omega}{\upsilon_f}}\,z\end{aligned}\right\}\tag{11}$$

where η is the non-dimensional distance along the axis of rotation. Further, F, G and θ are functions of η.

Taking help of eqs (7), (8), (9), (10) and (11), eqs (2), (3),(5) and (6) take the form

$$\left\{\frac{1}{(1-\phi)^{2.5}\left[(1-\phi)+\phi\left(\frac{\rho_s}{\rho_f}\right)\right]}\right\}\left(2F'''-KF'\right)$$
$$+2FF''-F'^2+G^2+\left\{\frac{(1-\phi)+\phi\left(\frac{(\rho\beta)_s}{(\rho\beta)_f}\right)}{(1-\phi)+\phi\left(\frac{\rho_s}{\rho_f}\right)}\right\}\left(\frac{G_r}{\mathrm{Re}^2}\right)\theta-F_rF'^2=0\tag{12}$$

$$\left\{\frac{1}{(1-\phi)^{2.5}\left[(1-\phi)+\phi\left(\frac{\rho_s}{\rho_f}\right)\right]}\right\}\left(G''-KG\right)$$
$$+2FG'-2F'G+\left\{\frac{(1-\phi)+\phi\left(\frac{(\rho\beta)_s}{(\rho\beta)_f}\right)}{(1-\phi)+\phi\left(\frac{\rho_s}{\rho_f}\right)}\right\}\left(\frac{G_r}{\mathrm{Re}^2}\right)\theta-F_rG^2=0\tag{13}$$

$$\frac{k_{nf}}{k_f}\left\{\frac{1}{(1-\phi)+\phi\left(\frac{(\rho C_p)_s}{(\rho C_p)_f}\right)}\right\}\theta''+\Pr F\theta'=0 \tag{14}$$

$$\left.\begin{aligned} F'=\gamma+\delta\Gamma F'', G=1+\delta\Gamma G', F=\Upsilon, \left(\frac{k_{nf}}{k_f}\right)\theta'=-B_i(1-\theta) \quad at\ \eta=0 \\ F'\to 0, G\to 0,\ \theta\to 0\ as\ \eta\to\infty \end{aligned}\right\} \tag{15}$$

where

$$\left.\begin{aligned} K=\frac{\upsilon_f}{\gamma K^*},\ G_r=\frac{g\beta_f(T_f-T_\infty)r^3}{\upsilon_f^2},\ \ \delta=\frac{1}{(1-\phi)^{2.5}} \\ F_r=\frac{C_d}{\sqrt{K^*}}, \Pr=\frac{\nu_f}{\alpha_f}, \gamma=\frac{S}{\Omega}, \Upsilon=\frac{W}{\sqrt{2\Omega\upsilon_f}} \\ \Gamma=L_1\mu_f\sqrt{\frac{2\Omega}{\upsilon_f}},\ B_i=\frac{h_f}{k_f}\sqrt{\frac{\upsilon_f}{2\Omega}}, \end{aligned}\right\} \tag{16}$$

Here K is the porosity parameter, Gr is the thermal Grashof number, δ is a non dimensional parameter, F_r is the inertia parameter, $\Pr$ is the Prandtl number, γ is the stretching strength parameter, Γ is the velocity slip parameter, Bi is the Biot number. $\Upsilon=\frac{W}{\sqrt{2\Omega\upsilon_f}}$ represents suction and injection according to $W>0$ and $W<0$ respectively.

The non-dimensional local skin friction coefficient can be formed as

$$(\mathrm{Re}_r)^{1/2}C_f=\frac{1}{(1-\phi)^{2.5}}\left\{\sqrt{\left[F''(0)\right]^2+\left[G'(0)\right]^2}\right\} \tag{17}$$

The non-dimensional local Nusselt number $(\mathrm{Re}_r)^{-1/2}Nu_r$ reads

$$\left(\mathrm{Re}_r\right)^{-1/2} Nu_r = -\left(\frac{k_{nf}}{k_f} + \frac{4}{3}Rd\right)\theta'(0) \tag{18}$$

3. Method of Solution

The governing equations are represented by a system of highly coupled equations (12)-(14) which are highly nonlinear and cannot be solved analytically. The governing equations form a two point boundary valued problem (BVP) together with the boundary condition (15) which can be solved using the routine bvp4c of the symbolic computer mathematical tools MATLAB (see Hemalatha et al. [43], salahuddin et al.[44] and Nayak et al. [45]) . In this routine, first convert the BVP into an initial values problem (IVP). To continue this process, we have to choose a finite value of the boundary $\eta \to \infty$, say η_∞ and the numerical value of this parameter depends on the other governing parameters which influence the present system.

4. Results and Discussion

The current study focuses on the flow and thermal characteristics of steady Darcy-Forchheimer flow of $Fe_3O_4 - (CH_2OH)_2$ nanofluid past a stretching/shrinking rotating disk subject to suction and velocity slip. The 4th order Runge-Kutta method has been implemented in accomplishing the desired solution the transformed non-linear coupled equations. Universal values of the parameters embedded in the present investigation are $Gr = 0.1, F_r = 0.1,$ $Pr = 7, \gamma = 0.5, \Gamma = 0.5, \delta = 0.5,$ $\mathrm{Re} = 1, \Upsilon = 0.5, B_i = 0.1$. The thermo-physical properties of the base fluid and the considered nanoparticles at T=300K are incorporated in Table 1. The outcomes of the velocity distribution, temperature distribution, skin friction and Nusselt number under the influence of pertinent parameters have been discussed through organized graphs and numerical tables. The present section comprises of a number of sub-sections accommodating velocity and temperature profiles, skin friction and Nusselt number variations.

4.1 Velocity Profiles

Analysis of velocity distribution $F'(\eta)$ in response to slip parameter Γ is displayed in Fig. 2. Higher values Γ lead to the upgradation of $F'(\eta)$ within $\eta = 1.5$ and beyond $\eta = 1.5$ variation of $F'(\eta)$ is marginal for stretching

rotating disk. On the other hand, incremented Γ declined the $F'(\eta)$ profiles thereby reducing the velocity boundary layer thickness. However, the reverse trend is the result in the flow due to shrinking rotating disk beyond $\eta = 1.5$. Fig. 3 evaluates the performance of tangential velocity $G(\eta)$ due to increment in Γ for both stretching and shrinking Darcy Forchheimer flow near the boundary $(\eta = 1.5)$. Beyond $\eta = 1.5$ flow due to shrinking rotating disk shows its prominence over the flow due to stretched rotating disk. The basic cause behind it is that enhancing the slip on the surface of the disk peters out the fluid stuck to it. The efficiency of the rotating disk then fritters away substantially and therefore could not deliver its circumferential momentum to the fluid particles concerned.

Fig. 4 delineates that increment in suction parameter Υ leads to the diminution of velocity field in the entire stretched flow domain. As a result, the velocity boundary layer shrinks. The cause for the decelerated flow is that suction brings the distance fluid into the region near to the surface of the disk which in turn augments the fluid viscosity. Consequently, the fluid motion retards. Further, rising Υ exhibits exactly the same behavior of $F'(\eta)$ for the flow due to shrinking rotating disk. However, the decline due to stretched flow is faster compared to shrinking flow in response to rising suction and also more fluid suction diminishes the tangential velocity $G(\eta)$ due to stretched flow (Fig. 5). Meanwhile, more suction yields diminutive $G(\eta)$ in case of flow due to shrinking rotating disk up to $\eta = 2$ and afterwards the behavior changes.

Fig. 6 demonstrates the variation of $F'(\eta)$ for varied stretching strength parameter γ. It is noticed that higher γ upsurges $F'(\eta)$ for the flow due to stretching rotating disk while that of γ imparts an opposite trend for the flow due to shrinking rotating disk within the few layers from the surface of the disk. It is pertinent to reveal here that an inverted boundary layer structure is developed due to the flow over a shrinking rotating disk. Such outcome is due to the fact that the free stream velocity is dominated by the angular velocity of the rotating disk. Fig. 7 portrays that incremented γ diminished $G(\eta)$ monotonically leading to thinner hydrodynamic boundary layer. However, significant descending trend of $G(\eta)$ is noticed due to flow over shrinking rotating disk. This is because increase in

stretching strength parameter decays the rotational velocity which in turn reduces the tangential velocity.

4.2 Temperature Profiles

Figs.8 and 9 reveal thermal characteristics of steady Darcy-Forchheimer flow of $Fe_3O_4-(CH_2OH)_2$ nanofluid past a stretching/shrinking rotating disk in presence of velocity slip and suction. The temperature field $\theta(\eta)$ declines due to augmentation in Υ for both stretching/shrinking rotating disk. Bringing the ambient fluid towards the surface of the solid rotating disk (stretching/shrinking) makes the nanofluid more viscous. Consequently, the fluid temperature gets escalated. However, the descending trend is more prominent for the flow over stretching rotating disk compared to the flow over shrinking rotating disk (Fig. 8). In addition, one observes that impact of fluid suction leads to the modification of thermal boundary layer structure for both the flow over stretching and shrinking rotating disk. Fig. 9 narrates that incremented γ upsurged $\theta(\eta)$ and the related boundary layer thickness for the flow due to both stretching and shrinking RD. For a certain γ, in case of shrinking rotating disk, as η rises $\theta(\eta)$ grows up to a maximum value $\theta_{\max}(\eta)$ at a particular η and decays with further rise in η. Temperature distribution $\theta(\eta)$ shows exactly opposite trend for both stretching and shrinking rotating disk (Fig. 9).

4.3 Variation of Skin friction and Local Nusselt Number

Table 2 conveys the variation of skin friction $\left(\mathrm{Re}^{\frac{1}{2}} C_f\right)$ and local Nusselt number $\left(\mathrm{Re}^{-\frac{1}{2}} Nu_r\right)$ for varied values of $Gr, K, \mathrm{Re}, Fr, \gamma, \Gamma, \delta, \Upsilon, B_i$. Rising Gr reduces $\mathrm{Re}^{\frac{1}{2}} C_f$ for stretching rotating disk while that of Gr upgrades $\mathrm{Re}^{\frac{1}{2}} C_f$ for shrinking rotating disk. The local Nusselt number $\left(\mathrm{Re}^{-\frac{1}{2}} Nu_r\right)$ peters out due to enhancement in thermal buoyancy (increasing Gr) while that decays in response to lower thermal buoyancy effect. This is because rising Gr makes thermal buoyancy force more than the viscous force.

Augmented porosity parameter K belittles $\mathrm{Re}^{\frac{1}{2}} C_f$ while that of Re enhances $\mathrm{Re}^{\frac{1}{2}} C_f$ for both flow over stretching and shrinking rotating disk. This implicates that presence of porous matrix influences the viscous drag force well for both rotating disk. It is important to mention here that introducing more porous matrix diminishes the absolute value of Nusselt number $\left(\mathrm{Re}^{-\frac{1}{2}} Nu_r \right)$ for stretching rotating disk. This is because the resistive force due to porous matrix restrains the flow velocity which in turn rises the temperature. Augmented Re diminishes heat transfer rate from the surfaces of stretching and shrinking rotating disk. The basic cause behind it is that increase in Reynolds number implicates domination of inertial force over viscous force lessens the flow velocity and therefore the elevation of fluid temperature. Greater slip causes reduction of viscous drag force for stretching rotating disk while a reverse outcome is accomplished due to shrinking rotating disk. Further, greater slip augments heat transfer rate for stretching rotating disk and diminishes due to shrinking rotating disk. Fluid suction uplifts $\mathrm{Re}^{\frac{1}{2}} C_f$ and heat transfer rate from the surface of the stretching rotating disk. Convective heat transfer strengthens viscous drag force ($\mathrm{Re}^{\frac{1}{2}} C_f$) while that peters out heat transfer rate for the flow over both stretching and shrinking rotating disk.

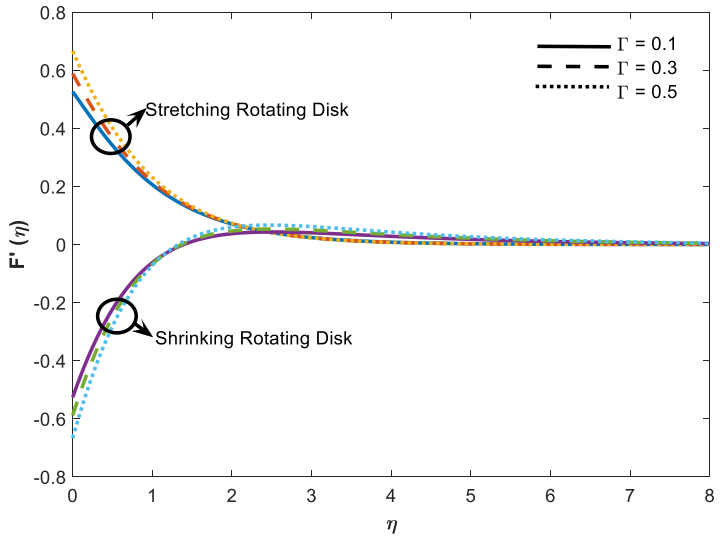

Fig. 2: Radial velocity profile for different Γ.

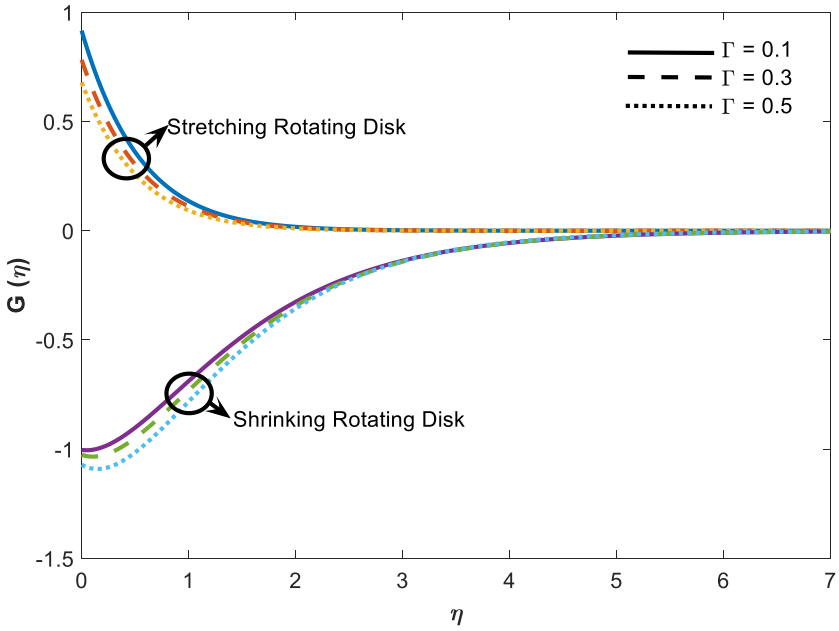

Fig. 3: Tangential velocity profile for different Γ.

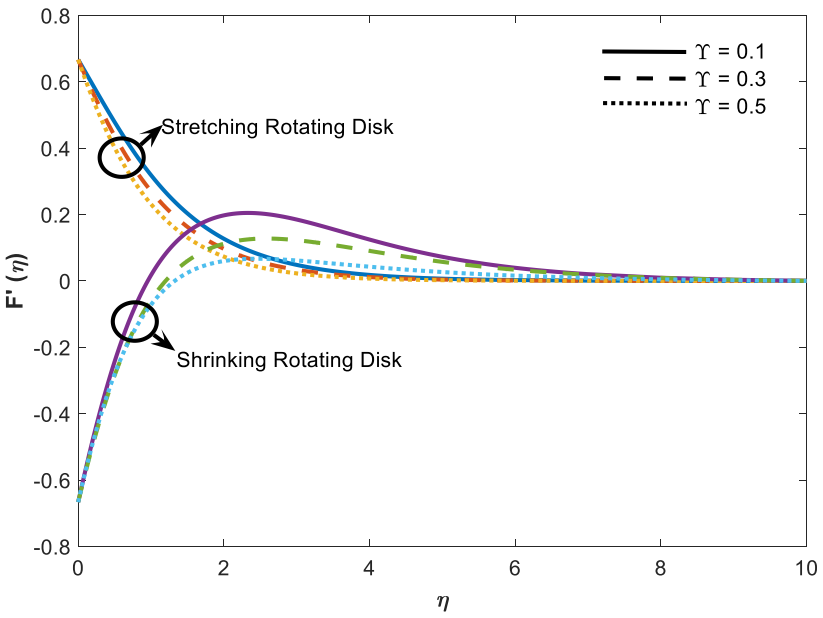

Fig. 4: Radial velocity profile for different ϒ.

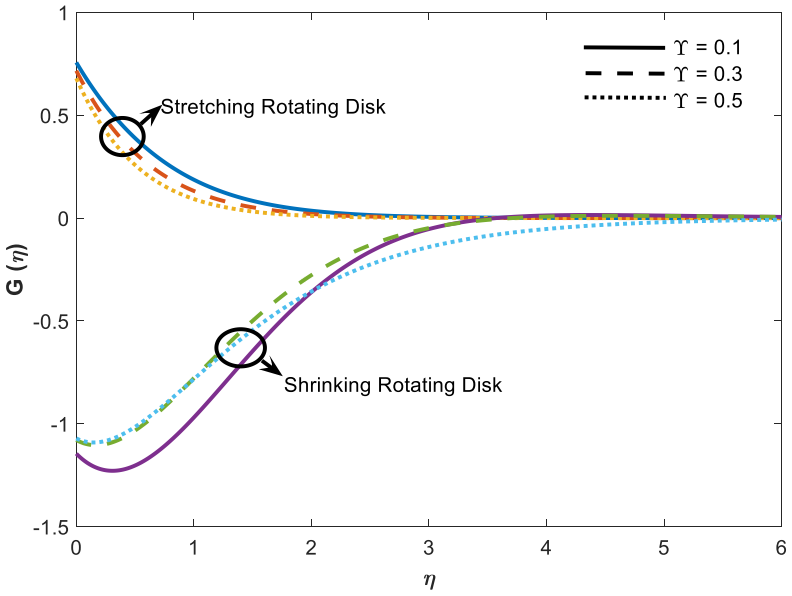

Fig. 5: Tangential velocity profile for different ϒ.

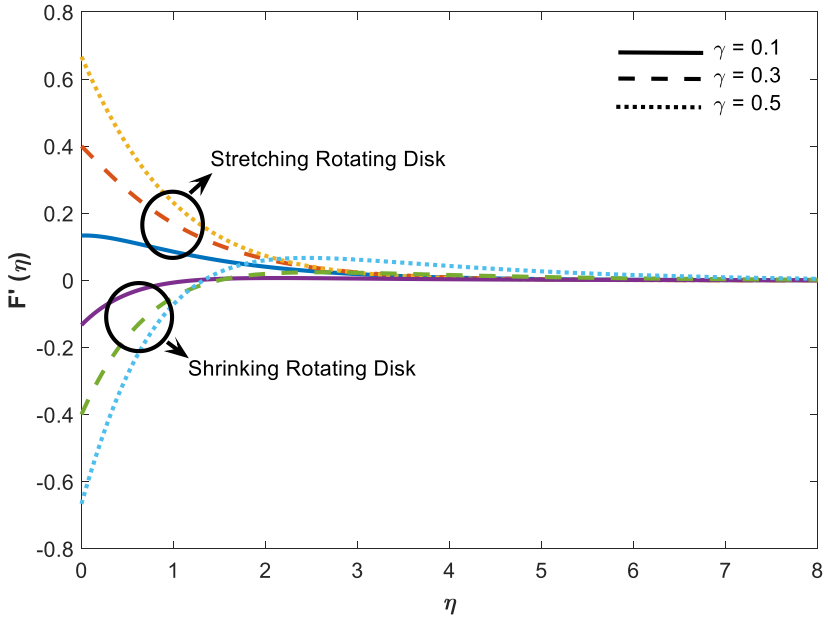

Fig. 6: Radial velocity profile for different γ.

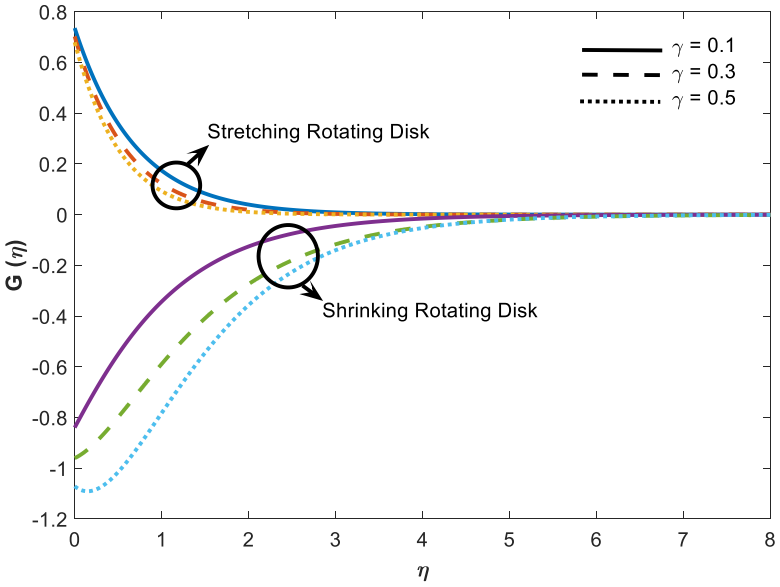

Fig. 7: Tangential velocity profile for different γ.

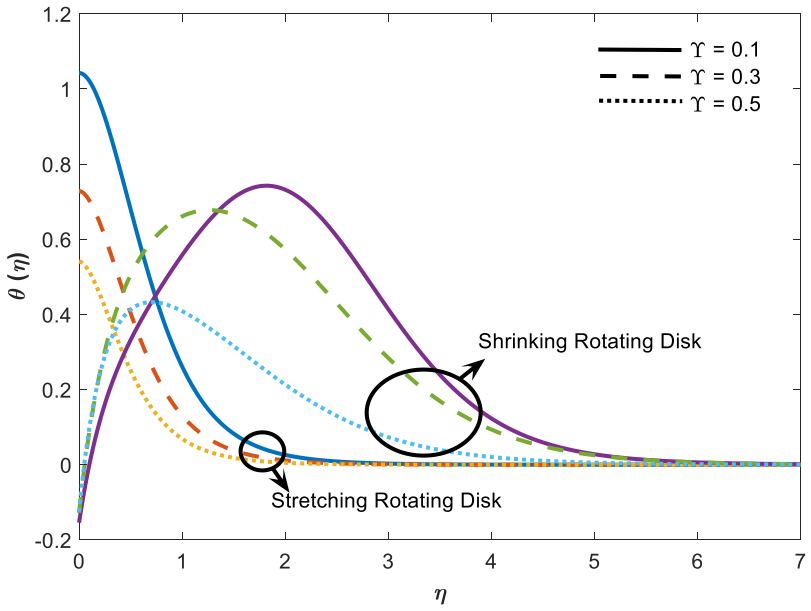

Fig. 8: Temperature profile for different ϒ .

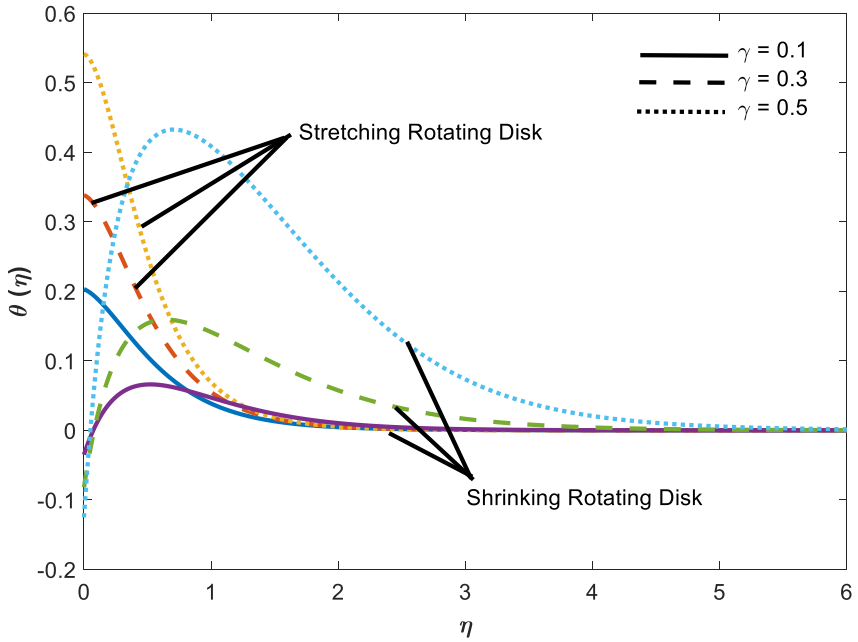

Fig. 9: Temperature profile for different γ.

Table 1. Thermo-physical properties of the base fluid and nanoparticles at T=300K.

	$\rho\ (Kg/m^3)$	$C_P\ (J/KgK)$	$k\ (W/mK)$	$\mu_f\ (Ns/m^2)$
Pure Water	997.1	4179	0.613	0.001003
$(CH_2OH)_2$ or $C_2H_6O_2$	1115	2430	0.253	
Fe_3O_4	5180	670	9.7	

Table 2. Skin friction and local Nusselt number number with respect to different parameters (first row for stretching disk and second row for shrinking disk).

Gr	K	Re	F_r	γ	Γ	δ	Υ	B_i	$Re_r^{1/2}C_f$	$Re_r^{-1/2}Nu_r$
0.1									1.42993	-3.35380
									1.59271	-4.83995
0.4									1.34438	-3.36250
									1.79190	-3.53124
0.7									1.23235	-3.40009
									2.53185	-3.52885
	0								1.43865	-3.39415
									1.21267	-4.62126
	0.2								1.42067	-3.31474
									1.89321	-5.13405
		1							1.45181	-2.58110
									2.34283	-5.36044
		2							1.45417	-2.19727
									2.48680	-5.27618
			0.1						1.39264	-3.37600
									0.79509	-4.45780
			0.3						1.41150	-3.36451
									0.98686	-4.51407
									1.34667	-8.16669
									1.53750	-10.92138
									1.25384	-13.19130
									1.99109	-18.18769
				0.1					1.06798	-1.43648
									0.43249	-0.68481
				0.3					1.23336	-2.23137

									0.81545	-2.18268
					0.1				1.74959	-3.44576
									1.31950	-3.38681
					0.3				1.54335	-3.28402
									1.43714	-3.99596
						0.1			1.74959	-3.44576
									1.31950	-3.38681
						0.3			1.54335	-3.28402
									1.43714	-3.99596
							0.1		1.12498	-2.69834
									1.86659	-3.11390
							0.3		1.27530	-3.03058
									1.60601	-4.03010
								0.5	1.48865	-7.36345
									1.18425	-4.54415
								0.8	1.53465	-10.47577
									2.04102	-10.04152
									1.43838	-3.48406
									1.66329	-4.61924
									1.44376	-3.56575
									1.71429	-4.59607

5. Concluding remarks

The present investigation deals with the flow and thermal characteristics of steady Darcy-Forchheimer flow of $Fe_3O_4-(CH_2OH)_2$ nanofluid past a stretching/shrinking rotating disk subject to suction, velocity slip and convective boundary condition. The major findings of the present study are:

- Higher velocity slip leads to diminution of tangential velocity due to stretching/shrinking rotating disk.

- Fluid suction diminishes the radial velocity and the related boundary layer thickness.
- Incremented γ augmented $\theta(\eta)$ and the related thermal boundary layer thickness due to both stretching and shrinking rotating disks.
- Rise in porosity parameter K decreases $\mathrm{Re}^{\frac{1}{2}} C_f$ while that of Re upsurges it for the flow over stretching and shrinking rotating disks.
- Larger Bi (more convective heat transfer) strengthens viscous drag force ($\mathrm{Re}^{\frac{1}{2}} C_f$) and peters out heat transfer rate from the surface of both stretching and shrinking rotating disks.

Reference

[1] S U S Choi, *ASME Fluids Eng. Division*, **231**, 99 (1995)

[2] A A Afify and N S Elgazery, *Particuology*, **29**, 154 (2016)

[3] T Hayat, M I Khan, A Alsaedi and M I Khan, *Int. Comm. Heat Mass Transf*., **89**, 190 (2017)

[4] M K Nayak, N S Akbar, V S Pandey, Z H Khan and D Tripathi, *Powder Technol*. **315**, 205 (2017)

[5] T Hayat, S Ahmad, M I Khan and A Alsaedi, *Phys. B: Cond. Matt*., **537**, 116 (2018)

[6] M K Nayak, *Int. J. Mech. Sci.* **125**, 185 (2017)

[7] A S Dogonchi and D D Ganji, *J. Taiwan Inst. Chem. Eng.* **80**, 52 (2017)

[8] M K Nayak, R Mehmood, O D Makinde, O Mahian and Ali J Chamkha, *J. Central South University*, **26**, 1146 (2019)

[9] M Mustafa, *Int. J. Heat Mass Transfer*, **108**, 1910 (2017)

[10] M K Nayak, S Shaw, V S Pandey and Ali J Chamkha, *Indian J. Phys***. 92**, 1017 (2018)

[11] T Von Kármán, *Z. Angew Math. Mech.* **1**, 233 (1921)

[12] M Turkyilmazoglu and P Senel, *Int. J. Thermal Sci*. **63**, 146 (2013)

[13] U T Bödewadt, *Z. Angew Math. Mech*. **20**, 241(1940)

[14] M Sheikholeslami, M. Hatami and D D Ganji, *J. Mol. Liq*. **211**, 577 (2015)

[15] S K Das, S U S Choi, W Yu and T Pradeep, *Wiley, New Jersey, USA*, (2007)

[16] D A Nield and A V Kuznetsov, *Int. J. Heat Mass Transf*. **52**, 5796 (2009)

[17] P Forchheimer, *Zeitschrift Ver. D. Ing*. **45**, 1782 (1901)

[18] M Muskat, *The Flow of Homogeneous Fluids Through Porous Media, Edwards, MI,* (1946)

[19] M A Seddeek, *J. Colloid Interface Sci*. **293**, 137 (2006)

[20] S A Shehzad, F M Abbasi, T Hayat and A Alsaedi, *J. Mol. Liq*. **224**, 274 (2016)